1 **Electronic Supplementary Information for**

2

3 **Revealing the multiple cathodic and anodic involved charge storage mechanism in a FeSe$_2$**

4 **cathode for aluminium-ion batteries by *in situ* magnetometry**

5 *Huaizhi Wang[a,‡], Linyi Zhao[a,‡], Hao Zhang[a], Yongshuai Liu[a], Li Yang[a], Fei Li[a], Wenhao Liu[a], Xiaotong*

6 *Dong[a], Xiangkun Li[a], Zhaohui Li[a], Xiaodong Qi[b], Langyuan Wu[b], Yunfei Xu[c], Yaqun Wang[c], Kuikui*

7 *Wang[a], Huicong Yang[d], Qiang Li[a,*], Shishen Yan[e], Xiaogang Zhang[b], Feng Li[d], and Hongsen Li[a,*]*

8

9 [a] College of Physics, Center for Marine Observation and Communications, Qingdao University,

10 Qingdao 266071, China. E-mail: hsli@qdu.edu.cn; liqiang@qdu.edu.cn

11 [b] Jiangsu Key Laboratory of Materials and Technologies for Energy Conversion, College of Material

12 Science and Engineering, Nanjing University of Aeronautics and Astronautics, Nanjing 210016,

13 China.

14 [c] College of Electrical Engineering and Automation, Shandong University of Science and

15 Technology, Qingdao 266590, China.

16 [d] Shenyang National Laboratory for Materials Science, Institute of Metal Research, Chinese

17 Academy of Sciences, Shenyang 110016, China.

18 [e] School of Physics, State Key Laboratory of Crystal Materials, Shandong University, Jinan 250100,

19 China.

20 [‡] H.W. and L.Z. contributed equally to this work.

21 * Corresponding authors

22

23

24

25

26

27

28

29

Experimental Section

Chemicals and materials: All chemicals were of analytical grade and use without further purification.

Preparation of Fe$_2$O$_3$: The Fe$_2$O$_3$ nanorods were synthesized by a hydrothermal method. Typically, 0.5 g of FeCl$_2$ was diluted with a mixed solution of ethyl alcohol and deionized water (1:1 v/v, 80 mL) in the formation of light brown solution under stirring. 0.3 g of Na$_2$C$_2$O$_4$ was then added to the above solution under stirring yielding a bright yellow suspension, transferring and sealing in a 100 mL Teflon-lined stainless steel autoclave and kept at 180°C/20 h. After cooling to room temperature, the precipitate was washed with distilled water and ethanol several times, dried at 60 °C in vacuum for 12 h. Finally, the product was annealed in air at 600°C for 3 h with a rate of 2°C min^{-1} to achieved brick-red Fe$_2$O$_3$ rods.

Preparation of FeSe$_2$: 30 mg of as-prepared Fe$_2$O$_3$ was mixed with selenium powder in a mass ratio of 1:10, which was then put into a combustion boat and covered with a glass plate. Subsequently, the combustion boat was placed in a tube furnace and calcinated at 400 °C for 10 h under a flow of 5% Ar/H$_2$ gas with a temperature ramp of 1 °C min^{-1}.

Preparation of FeSe$_2$@GO: 10 mg of graphene oxide (GO, provided by Tanfeng Tech.Inc.) was mixed with 10 mL of deionized water and sonicated for 3 h. After that, 20 mg of FeSe$_2$ was added to 20 mL of water, and then, the as-prepared GO suspension was slowly poured into it. After sonicating for 10 min, the solution was stirring for another 12 h. At last, the black sample was collected by centrifugation with deionized and drying at 70 °C overnight, the rod-shaped FeSe$_2$@GO composite was obtained.

Materials characterizations: The as-prepared samples were characterized on an XRD (Bruker D8 Advance, Germany) equipped with a Cu Kα radiation source at 40 kV and 30 Ma. XPS was performed on an ESCALAB250Xi X-ray photoelectron spectrometer, studying the surface chemical composition and valent state of the element of the products. FESEM (ZEISS, Sigma 500) and TEM (JEOL, JEM-2100F) were carried out to analyze the morphology. Raman spectra were conducted using a LabRAM HR Evolution Raman spectrophotometer (HORIBA JY). *In situ* Raman spectra were accomplished by ThermoFisher Scientific-DXR2 Raman microscope with an excitation laser wavelength of λ=532 nm.

Electrochemical measurements: The storage properties of the AIBs were researched by pouch cells in an argon-filled glovebox (O$_2$ < 0.01 PPm, H$_2$O < 0.01 PPm). To fabricate the cathode, the FeSe$_2$@GO composite was mixed with conductive carbon black (Super P, 20 wt%) and binder (polyvinylidene

1   fluoride (PVDF) in N-methyl-pyrrolidone (NMP) with a mass ratio of 7:2:1, which was then coated

2   on a molybdenum foil current collector with 0.03 mm in thickness. The prepared electrode was further

3   dried at 60 ℃ for 12 h. At the same time, aluminium foil (99.99%) acted as the anode. Notably, ionic

4   liquid electrolyte (ILs) electrolyte of $AlCl_3$/[EMIm]Cl with ratio of 1.3:1 and Whatman GF/C type

5   glass fiber paper was used as electrolyte and separator, respectively. The galvanostatic charge-

6   discharge tests of the AIBs were measured over a voltage range of 0.01-2.2 V (*vs*. Al/Al^{3+}) on a Neware

7   battery cycler (CT-4008T-5V20 mA-164, Shenzhen, China). The CV curves were evaluated on an

8   Al//$FeSe_2$@GO cell at a scan of 0.5 mV s^{-1} using an electrochemical workstation (IVIUM technologies,

9   Vetex. One. EIS). The electrochemical impedance spectroscopy was also carried out by using an

10 electrochemical workstation (IVIUM technologies, Vetex. One. EIS) at ambient temperature.

11 *Magnetic characterization:* The AIBs for the *in situ* magnetometry test were assembled by using a

12 pouch-type cell in an argon-filled glovebox at room temperature. The operando measurements were

13 performed in a Quantum Design physical property measurement system (PPMS) magnetometer at a

14 temperature of 300 K. Simultaneously, the $FeSe_2$@GO AIBs were connected in galvanostatic mode at

15 1 A g^{-1} from 0.01 to 2.2 V while the magnetization was sampled at constant field (3 T). The magnetic

16 fields were parallel to the molybdenum foil. Magnetic hysteresis (MH) curves on electrode materials

17 were taken with *ex situ*, electrodes were washed in the glovebox after discharged to 0.01 V to avoid

18 oxidation.

19 *Theoretical calculation:* The First-principle calculation[1, 2] was conducted to perform all Spin-

20 polarization density function theory (DFT) using the Vienna Ab initio Simulation Package (VASP).

21 The exchange correlation potential was built using generalized gradient approximation (GGA) of the

22 Perdew-Burke-Ernzerhof (PBE)[3] formulation. The projected augmented wave (PAW) potentials[4, 5]

23 have been chosen to describe the ionic cores and take valence electrons into account using a plane

24 wave basis set with a kinetic energy cutoff of 450 eV. Partial occupancies of the Kohn−Sham orbitals

25 were allowed using the Gaussian smearing method and a width of 0.05 eV. The electronic energy was

26 considered self-consistent when the energy change was smaller than 10^{-6} eV. A geometry optimization

27 was considered convergent when the energy change was smaller than 0.05 eV $Å^{-1}$. In addition, for the

28 Fe atoms, the U schemes need to be applied, and the U has been set as 3.2 eV. Finally, the binding

29 energies(Eads)[6] were calculated as Eads=Ead/sub-Ead-Esub, where Ead/sub, Ead, and Esub are the

30 total energies of the optimized adsorbate/substrate system, the adsorbate, and the clean substrate,

1 respectively.
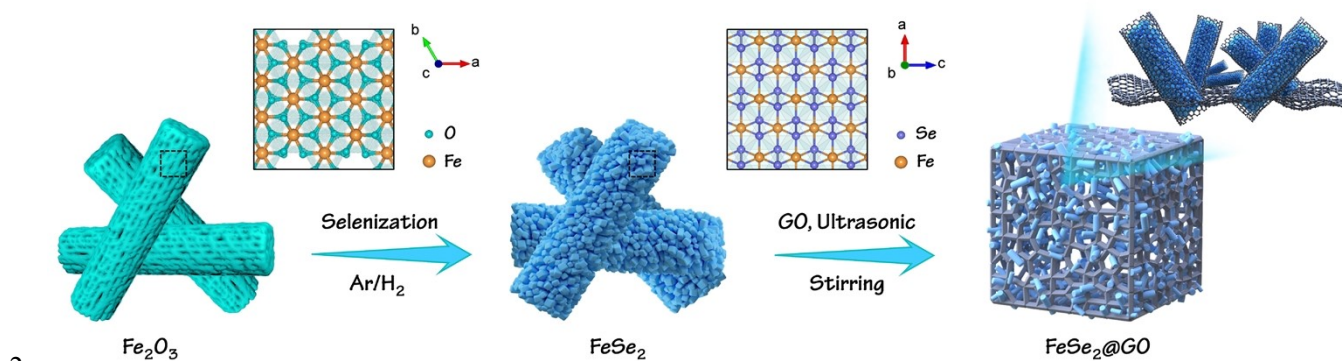
3 **Fig. S1.** Schematic illustration for the synthesis of the rod-shaped FeSe$_2$@GO.

4   Firstly, a porous Fe$_2$O$_3$ precursor was synthesized through a hydrothermal method using FeCl$_2$

5 and Na$_2$C$_2$O$_4$, followed by a calcining process in air to completely convert to pure Fe$_2$O$_3$. Subsequently,

6 the as-prepared Fe$_2$O$_3$ was calcinated in Ar/H$_2$ with excess selenium powder to obtain the desired FeSe$_2$

7 phase. Finally, the FeSe$_2$@GO composite was harvested by mixing a pre-dispersed GO with FeSe$_2$.

8

9

10

11

12

13

14
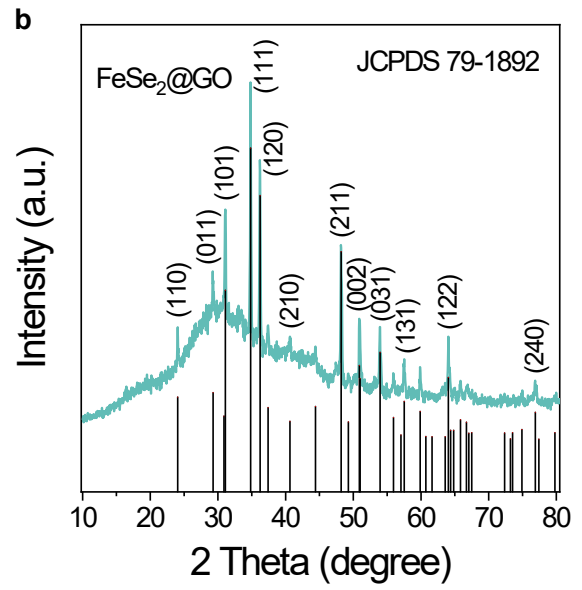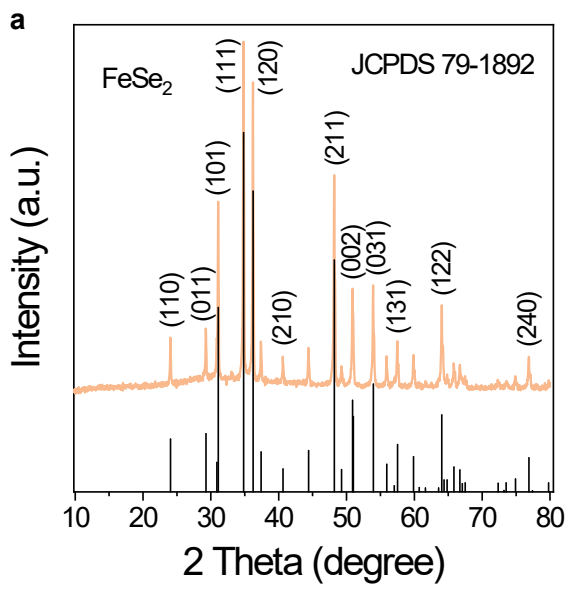
Fig. S2. XRD patterns of as-prepared $FeSe_2$ and $FeSe_2$@GO composite. XRD pattern of (a) bare $FeSe_2$, and (b) $FeSe_2$@GO composite.
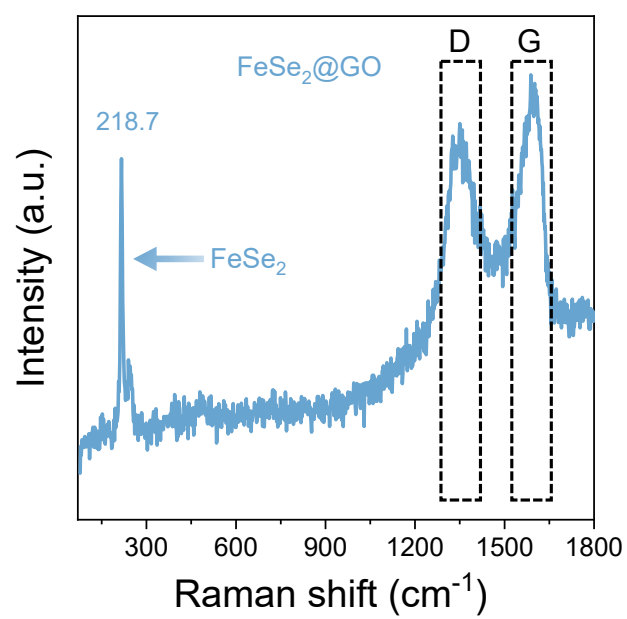
Fig. S3. Raman spectra of FeSe$_2$@GO composite.
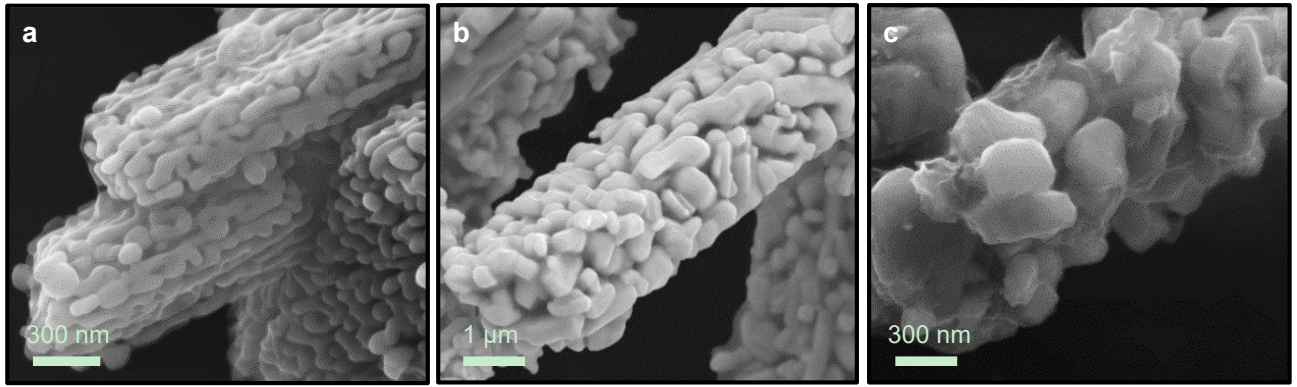
Fig. S4. FESEM images of the as-prepared materials. FESEM images of (a) Fe_2O_3, (b) bare $FeSe_2$, and (c) $FeSe_2$@GO composite.
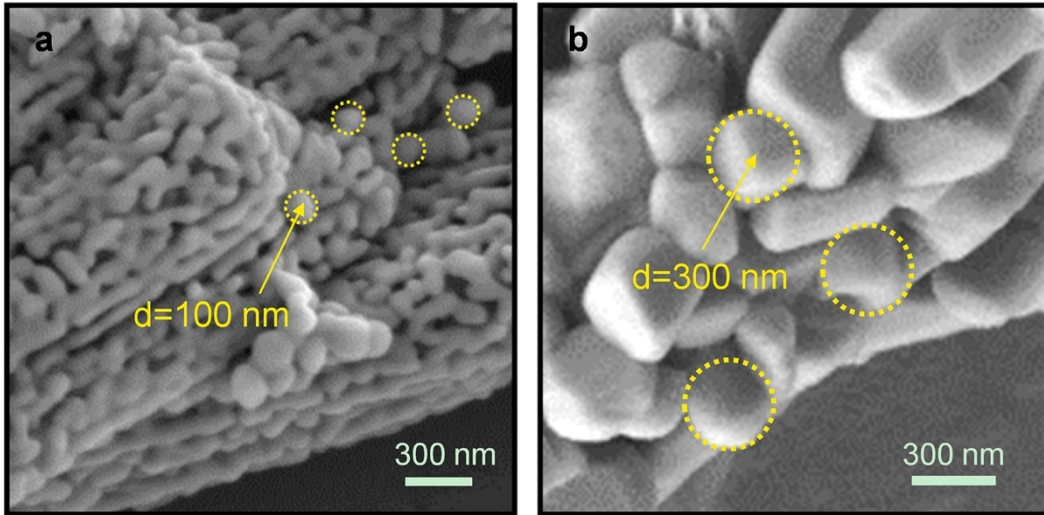
Fig. S5. The size of Fe_2O_3 and $FeSe_2$ particles. FESEM images of (a) Fe_2O_3 particles, and (b) $FeSe_2$ particles.

Fig. S6. TEM image of the FeSe$_2$@GO composite.

1
2
3
4
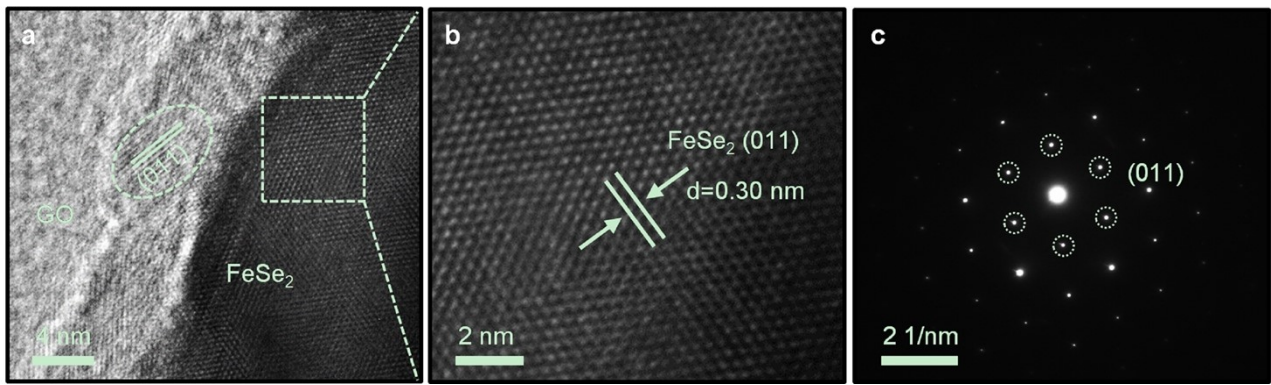5
6
7
8
9
10
11
12
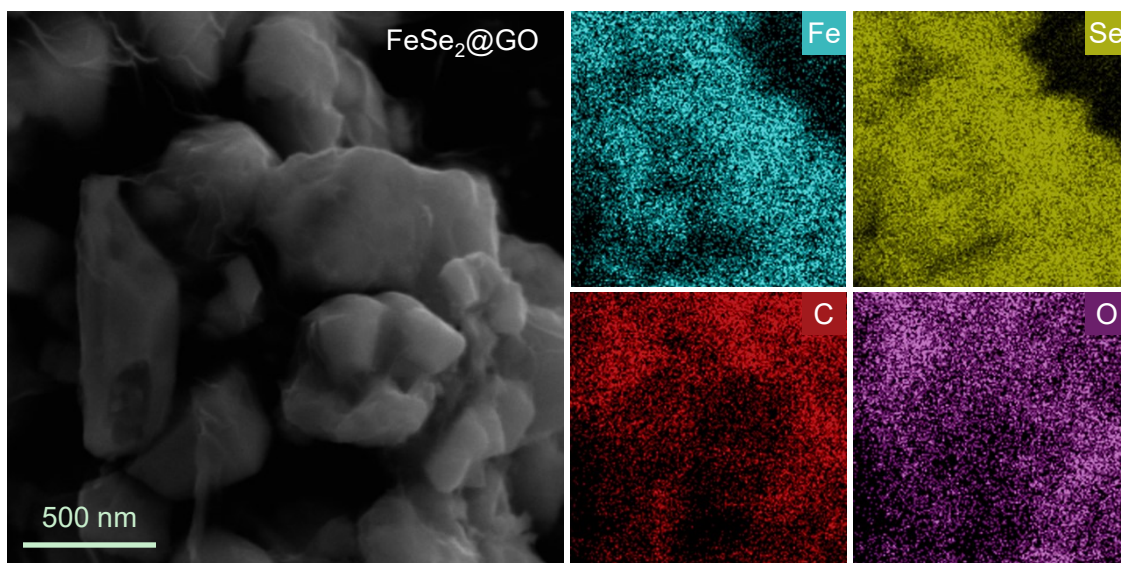13
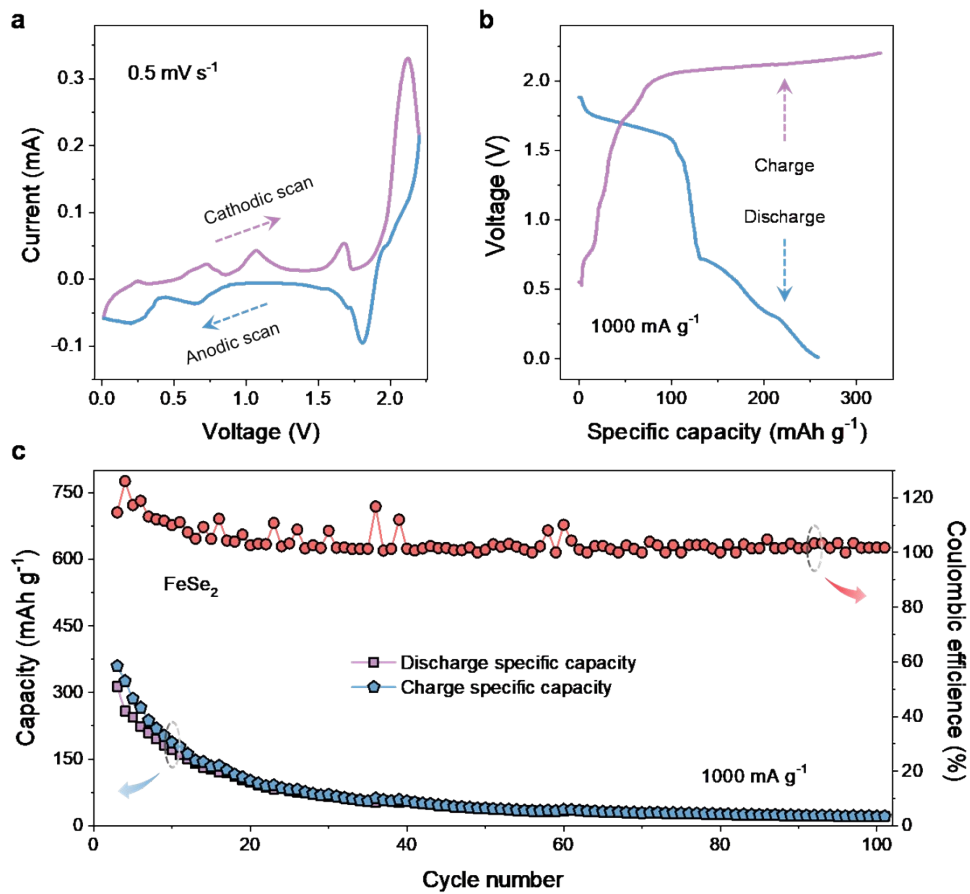14
15
16
17
18
19
20
21
22
23
24
25
26
27
28

Fig. S7. HRTEM images and SAED pattern of the FeSe$_2$@GO composite. (a) HRTEM image of the rod-shaped FeSe$_2$@GO composite. (b) the enlarged view of the dotted area in a. (c) SAED pattern of the FeSe$_2$@GO composite.

Fig. S8. EDS mapping of FeSe$_2$@GO composite.

1
2
3
4
5
6
7
8
9
10
11
12
13
14
15
16
17
18
19
20
21
22

23

Fig. S9. Electrochemistry of bare FeSe$_2$ in AIBs. (a) CV curves of FeSe$_2$ at a scan rate of 0.5 mV s^{-1}. (b) Charge-discharge curves of FeSe$_2$ at a current density of 1 A g^{-1}. (c) Cycling stability of FeSe$_2$ at a current density of 1 A g^{-1}.
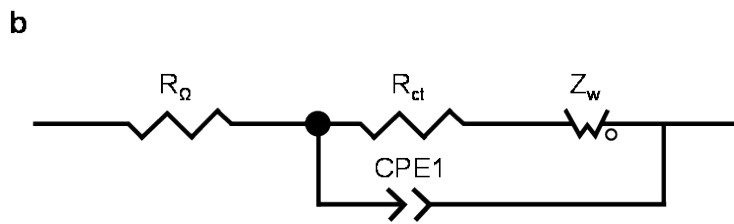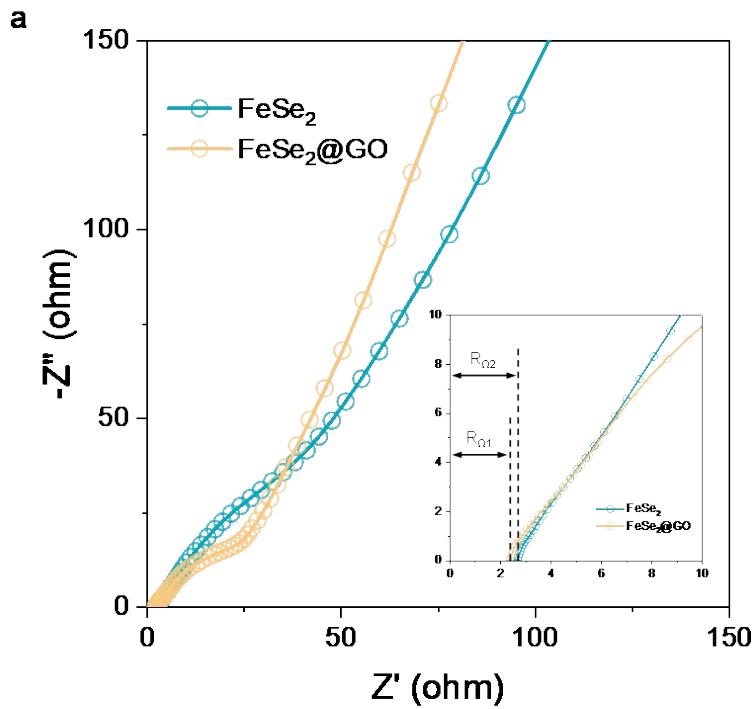
Fig. S10. Electrochemical impedance spectra of FeSe$_2$-based cathodes in AIBs. (a) The electrochemical impedance spectra of pure FeSe$_2$ and FeSe$_2$@GO composite (inset: enlarged plots) and (b) equivalent circuit model of the studied system.
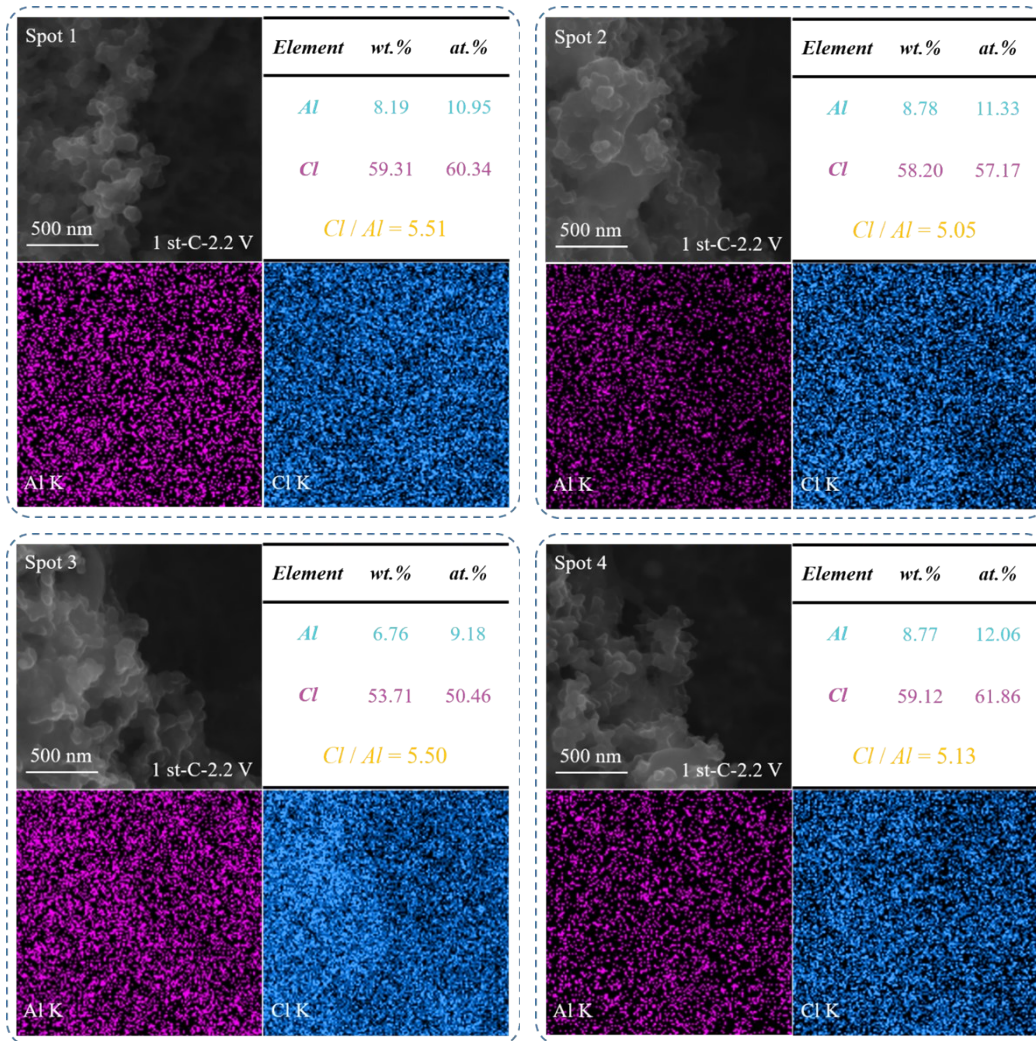
The ohmic resistance R$_\Omega$ (ohm) of FeSe$_2$@GO (2.213 Ω) and bare FeSe$_2$ (2.503 Ω) are at nearly the same levels, while the charge transfer resistance R$_{ct}$ (ohm) of FeSe$_2$@GO (39.23 Ω) is lower than that of bare FeSe$_2$ (107.7 Ω).
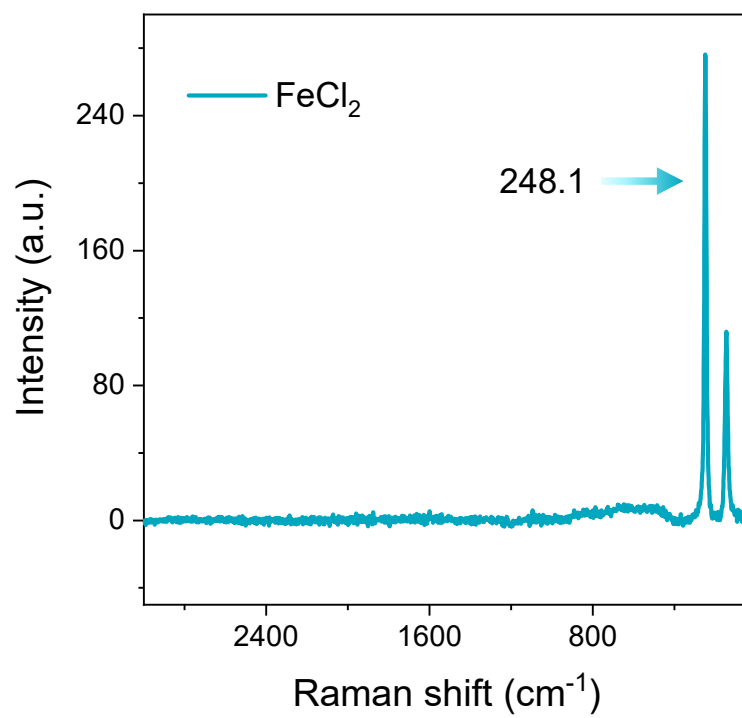
Fig. S11. Raman spectra of commercial FeCl$_2$ powder.

Fig. S12. EDS mapping of the first fully charged FeSe$_2$ at different spots.

1 **Table S1** Comparative electrochemical performance of FeSe$_2$@GO with other cathodes for AIBs
2 recently reported.
3

Cathode	Electrolyte (molar ratio)	Discharge capacity (mAh g^{-1})	Cycle number	Current density (mA g^{-1})	Discharge voltage (V)	Ref.
FeSe$_2$@GO	AlCl$_3$:[EMIm]Cl (1.3:1)	145	500	1000	1.84	This work
SnSe	AlCl$_3$:[EMIm]Cl (1.3:1)	80	200	300	1.62	7
G-SnS$_2$	AlCl$_3$:[EMIm]Cl (1.3:1)	70	100	200	0.68	8
CoS$_2$@CNFs	AlCl$_3$:[EMIm]Cl (1.3:1)	80	500	200	0.88	9
CuS@C	AlCl$_3$:[EMIm]Cl (1.3:1)	90	100	20	1.0	10
VS$_4$ nanowire clusters	AlCl$_3$:[EMIm]Cl (1.3:1)	98.66	250	800	0.54	11
MoS$_2$/CNFs	AlCl$_3$:[EMIm]Cl (1.3:1)	126.6	200	100	0.8	12
WS$_2$@NCNFs	AlCl$_3$:[EMIm]Cl (1.3:1)	195.81	100	100	0.8	13
C/V$_2$O$_5$	AlCl$_3$:[EMIm]Cl (1.3:1)	4	20	100	1.6	14
CoFe$_2$O$_4$@rGO	AlCl$_3$:[EMIm]Cl (1.3:1)	67	500	1000	0.4	15
Polythiophene	AlCl$_3$:[EMIm]Cl (1.5:1)	70	100	16	0.8-2.0	16
Polypyrrole	AlCl$_3$:[EMIm]Cl (1.5:1)	50	100	20	0.8-2.0	16
PTh/G-1:1	AlCl$_3$:[EMIm]Cl (1.3:1)	113.5	200	1000	0.5	17
Carbon paper	AlCl$_3$:[EMIm]Cl (1.3:1)	62	50	150	1.8	18

4
5
6
7
8
9
10
11
12
13

Table S2 Calculated lattice parameters, volume, total energy, and binding Energy for $FeSe_2$, $FeSe_2$ Al,
$FeSe_2$ ($AlCl_4$), and $FeSe_2$ Cl

Structure	a (Å)	b (Å)	c (Å)	Volume (Å)	Total Energy (eV)	Binding Energy (eV)
$FeSe_2$	3.631	4.818	5.793	101.378	-131.739	------
$FeSe_2$ Al	3.793	5.018	5.972	454.846	-201.997	-2.917
$FeSe_2$ ($AlCl_4$)	4.072	5.077	6.371	129.851	-293.574	-1.862
$FeSe_2$ Cl	3.681	4.953	5.931	108.133	-156.724	-2.751

References

1. J. F. G. Kresse, *Comp. Mater. Sci*, 1996, **6**, 15-50.

2. J. F. b. G. Kresse, *Phys. Rev. B*, 1996, **54**, 11170-11186.

3. K. B. John P. Perdew, Matthias Ernzerhof, *Phys. Rev. Lett.*, 1996, **77**, 3865-3868.

4. J. F. b. G. Kresse, *Phys. Rev. B*, 1999, **59**, 1758-1775.

5. P. E. Blochl, *Phys Rev B Condens Matter*, 1994, **50**, 17953-17979.

6. S. Grimme, J. Antony, S. Ehrlich and H. Krieg, *J. Chem. Phys.*, 2010, **132**, 154104.

7. Y. Zhang, B. Zhang, J. Li, J. Liu, X. Huo and F. Kang, *Chem. Eng. J.*, 2021, **403**, 126377.

8. Y. Hu, B. Luo, D. Ye, X. Zhu, M. Lyu and L. Wang, *Adv. Mater.*, 2017, **29**, 1606132.

9. R. Zhuang, Z. Huang, S. Wang, J. Qiao, J.-C. Wu and J. Yang, *Chem. Eng. J.*, 2021, **409**, 128235.

10. S. Wang, S. Jiao, J. Wang, H.-S. Chen, D. Tian, H. Lei and D.-N. Fang, *ACS Nano*, 2017, **11**, 469-477.

11. L. Xing, K. A. Owusu, X. Liu, J. Meng, K. Wang, Q. An and L. Mai, *Nano Energy*, 2021, **79**, 105384.

12. W. Yang, H. Lu, Y. Cao, B. Xu, Y. Deng and W. Cai, *ACS Sustainable Chem. Eng.*, 2019, **7**, 4861-4867.

13. W. Yang, H. Lu, Y. Cao and P. Jing, *J. Power Sources* 2019, **441**, 227173.

14. N. Canever and T. Nann, *Nano Ex.*, 2020, **1**, 010016.

15. K. Zhang, T. H. Lee, J. H. Cha, H. W. Jang, J.-W. Choi, M. Mahmoudi and M. Shokouhimehr, *Sci. Rep.* , 2019, **9**, 13739.

16. N. S. Hudak, *J. Phys. Chem. C.*, 2014, **118**, 5203-5215.

17. S. Zhao, H. Chen, J. Li and J. Zhang, *New J. Chem.*, 2019, **43**, 15014-15022.

18. H. Sun, W. Wang, Z. Yu, Y. Yuan, S. Wang and S. Jiao, *Chem. Commun.*, 2015, **51**, 11892-11895.